Contents lists available at ScienceDirect

Transactions of Nonferrous Metals Society of China

36(2026) 754−765

www.tnmsc.cn

Phase transformation and formation of lamellar structure in as-forged β-solidifying high Nb-containing TiAl alloy during annealing

Geng-wu GE, Lai-qi ZHANG *, Jun-pin LIN

State Key Laboratory for Advanced Metals and Materials, University of Science and Technology Beijing, Beijing 100083, China

Abstract: The elimination of the B2 phase in a β-solidifying high Nb-containing TiAl alloy with β/B2 and γ phases was investigated using different heat treatments, with a focus on understanding the phase transformations and lamellae formation during the process. The phase transformation and lamellae formation during B2 phase elimination differs from that observed in conventional TiAl alloys. During the holding stage of heat treatment, the β/B2 phase is replaced by the α phase through primary phase transformations of $\beta\rightarrow\alpha$ and $\gamma\rightarrow\alpha$. Lamellae formation occurs within both α and γ grains during cooling, initiating 30−40 °C below the annealing temperature. This lamellar structure was formed via two main mechanisms: nucleation at grain boundaries followed by growth into the grain, and direct precipitation and growth within the grain. The orientation relationship between the γ phase and its adjacent α phase is $(111)_\gamma//(0001)_\alpha$ and $[01\bar{1}]_\gamma//[11\bar{2}0]_\alpha$, with a coherency between the phases characterized by a misfit of approximately 1.7%.

Keywords: β-solidifying high Nb-containing TiAl; heat treatment; phase transformation; lamellar structure

1 Introduction

TiAl-based alloys are gaining popularity among researchers owing to their potential as next generation high-temperature structural materials, particularly for aerospace applications [1−4]. The alloys exhibit excellent high-temperature performance; however, their limited formability remains a challenging factor hindering their broader applications. Recently, in pursuit of improving high-temperature processing capabilities, research efforts have shifted towards β-solidifying γ-TiAl alloys, which offer improved high-temperature deformability compared to traditional γ-TiAl alloys [5−7]. The β phase within these alloys enhances the deformability at elevated temperatures. However, its corresponding ordered B2 phase at room temperature is brittle, necessitating strategies to minimize or eliminate it for enhanced room-temperature plasticity and high-temperature performance.

During the heat treatment process to reduce or eliminate the B2 phase, phase transformations and the development of lamellar structure are crucial. The microstructure significantly influences the mechanical properties of TiAl-based alloys. A duplex microstructure, comprising an equal amount of γ grains and lamellar structure, possesses good room-temperature plasticity, while a fully lamellar structure exhibits high strength and toughness [8]. Therefore, understanding the phase transformation during heat treatments is crucial for obtaining the desired microstructure [9−11]. LI et al [12] studied the phase transformation behavior and kinetics of high Nb−TiAl alloy under various cooling rates, finding that the fraction of phases depended on the cooling rate, and the lamellar structure formed when the cooling rate ranged from 3 to 40 °C/min. Notably, the lamellar colony size and interlamellar spacing decreased with fast cooling rates, contributing to

Corresponding author: *Lai-qi ZHANG, Tel: +86-13552059009, E-mail: zhanglq@ustb.edu.cn
https://doi.org/10.1016/S1003-6326(25)66995-0
Received 24 July 2024; accepted 16 January 2025

refined microstructures. By in-situ observation of β to α phase transformation in a β-solidifying TiAl alloy, KLEIN et al [13] indicated that α phase nucleated at grain boundaries, triple points, and pre-existing particles during the cooling process from the single β phase region, which is beneficial for microstructural refinement. QIANG et al [14] reported that the β_o phase precipitated in the α_2 lamellae in the aging process, with the $\alpha_2 \rightarrow \gamma$ transformation promoting the precipitation of β_o phase; however, β_o precipitate inhibits the $\alpha_2 \rightarrow \gamma$ transformation process. The formation of the lamellar structure in TiAl alloys with $\alpha+\gamma$ phases but without high Nb content has also been studied [15,16], and found formation pathways like: $\alpha \rightarrow \gamma \rightarrow \alpha_2 \rightarrow \alpha_2+\gamma$ or $\alpha \rightarrow \alpha_2 \rightarrow \alpha_2+\gamma$. However, these studies only focus on the traditional TiAl alloys containing γ, α_2, and β/B2 phases. It is worth noting that studies on the phase transformation and lamellae formation in TiAl alloy with the $\gamma+\beta$ microstructure remain limited.

Our previous research focused on forging of high Nb-containing $\beta-\gamma$ TiAl alloys that consist of β and γ phases, without the α_2 phase. This study leveraged the superior deformability of the β phase, enabling non-canned forging [17]. However, the B2 phase was found to adversely affect the mechanical properties. In this study, the elimination of the B2 phase is studied. Unlike previous work, this study specifically considers an alloy containing γ and β/B2 phases, aiming to elucidate the elimination of the β phase, phase transformation, and the formation mode of the lamellar structure in an as-forged β-solidifying high Nb-containing TiAl alloy through annealing, addressing a research gap in current research. The findings of this study will provide valuable guidance on microstructure control and the enhancement of mechanical properties of β-solidifying TiAl alloys.

2 Experimental

An as-forged β-solidifying high Nb-containing TiAl alloy with a nominal composition of Ti−44Al−8Nb−1.5Mn−1.0Cr−0.2B−0.2Y [18] was utilized to investigate the β phase elimination, phase transformation, and lamellar structure formation. The alloy, which exhibits excellent high-temperature deformability, can be forged without canning. For annealing, the specimens were heated to 1290 °C for a designated time period, followed by furnace cooling (FC) at a rate of 5 °C/min to a required temperature. Additionally, some specimens were water quenched (WQ) to preserve the microstructure for analysis of phase transformation.

High temperature laser-scanning confocal microscopy (HTLSCM, Lasertec VL2000DX-SVF17SP) was used to observe phase transformation and lamellar structure formation in real time. For this, a specimen measuring d7.5 mm × 3 mm was placed in an alumina ceramic crucible and heated to 1290 °C at a heating rate of 60 °C/min. After holding this temperature for 35 min, it was cooled to 1190 °C at a cooling rate of 5 °C/min, and then rapidly cooled to room temperature at a cooling rate of 300 °C/min.

The Vienna ab initio simulation package (VASP) was utilized to calculate the formation energy of the γ, α and β phases, based on the unit cell models with full optimization of cell shape, volume, and atomic positions using a cut-off energy of 450 eV.

Phase analysis was conducted using X-ray diffraction (XRD, Rigaku TTR3) with Cu K_α radiation over a 2θ range of 10°−90°. The microstructures were characterized before and after heat treatment using scanning electron microscopy (SEM, Zeiss Supra55) in backscattered mode. For detailed analysis of phase transformation and the lamellar structure, electron backscattered diffraction (EBSD, Oxford) and transmission electron microscopy (TEM, FEI TecnaiF30) were utilized. EBSD specimens were electro-polished in a solution containing 60% methanol, 35% *n*-butanol, and 5% perchloric acid by volume at −30 to −20 °C. TEM samples were prepared using two-jet electro-polishing in the same solution, and identical temperature and voltage conditions. Transmission Kikuchi diffraction (TKD) was applied on TEM specimen to analyzing the misorientation, crystallography relationship and phase transformation in the lamellar structure. The EBSD and TKD data were analyzed by Channel5 software and MTEX toolbox [19].

3 Results and discussion

3.1 As-forged microstructure

The microstructure of the as-forged β-solidifying high Nb-containing TiAl alloy is shown in Fig. 1. The wrought microstructure consists of γ and β phases without α_2 phase, and it is consistent

with XRD result. This absence is attributed to the incorporation of β-stabilizing elements such as Nb, Mn, and Cr. The volume fractions of the γ and β phases are 82% and 18%, respectively. Similarly, the as-cast microstructure also consists of γ and β phases, although the volume fraction of the β phase slightly increases after forging [17]. Additionally, some bright white particles, identified as Y_2O_3 are observed within the microstructure, due to the addition of Y element.

3.2 Elimination and phase transformation of β/B2 phase

To improve the mechanical properties of the as-forged β-solidifying high Nb-containing TiAl alloy, eliminating the β/B2 phase is essential. As depicted in Fig. 2(a), the microstructure of the specimen heated at 1290 °C for 6 h and subsequently quenched in water reveals equiaxed α_2 and γ grains, with the absence of the β/B2 phase. This result demonstrates that the β/B2 phase was successfully eliminated during the holding process, which is further supported by the XRD pattern shown in Fig. 2(b).

To identify the optimal temperature for effectively eliminating the β/B2 phase, the relationship between the heat treatment temperature and phase transformation time was examined. Figure 3 shows the water-quenching (WQ) micro-structures following heat treatment of specimen at various temperatures. After holding at 1210 °C for 12 h, some α phases begin to appear, though residual β/B2 phase remains in the microstructure. Increasing the temperature to 1230 °C allows for the full transformation of the β/B2 phase to the α phase within 9 h. Further temperature increase accelerates this process, requiring only 3 h at 1250 °C and just 2 h at 1270 °C. These results indicate that the time of phase transformation decreases as the heat treatment temperature increases, and lower temperatures are less conducive to phase transformation and the elimination of the β/B2 phase. The presence of significant amounts of β-stabilizing elements, such as Nb, Mn, and Cr, contributes to the β/B2 phase's resistance to transformation [20,21]. Therefore, annealing at temperatures higher than 1250 °C is more effective for eliminating the β/B2 phase due to the shortened transformation time.

To study the mechanism behind the elimination of the β phase, the specimen was heated at 1290 °C for 10 min, followed by furnace cooling to room temperature. The corresponding microstructure and phase map are shown in Fig. 4. The result indicates that the α phase nucleates at the γ/β interface, while no α phase forms at the grain boundary of the γ grains, suggesting that the γ/β interface is the preferred site for the nucleation of the α phase. This preference is

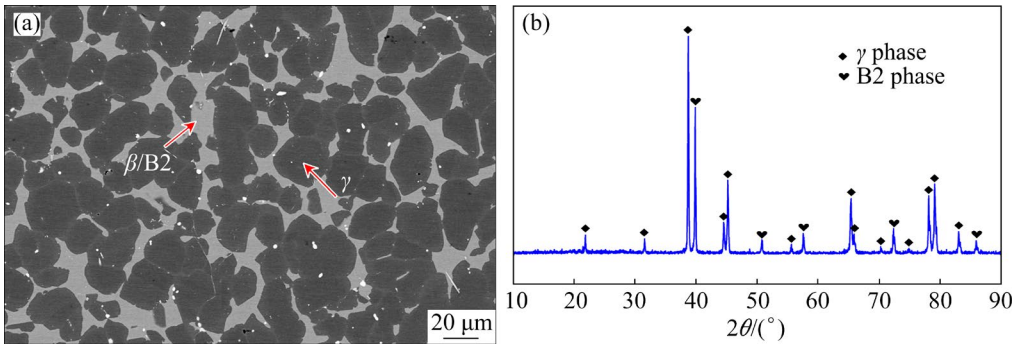

Fig. 1 Microstructure (a) and XRD pattern (b) of as-forged alloy

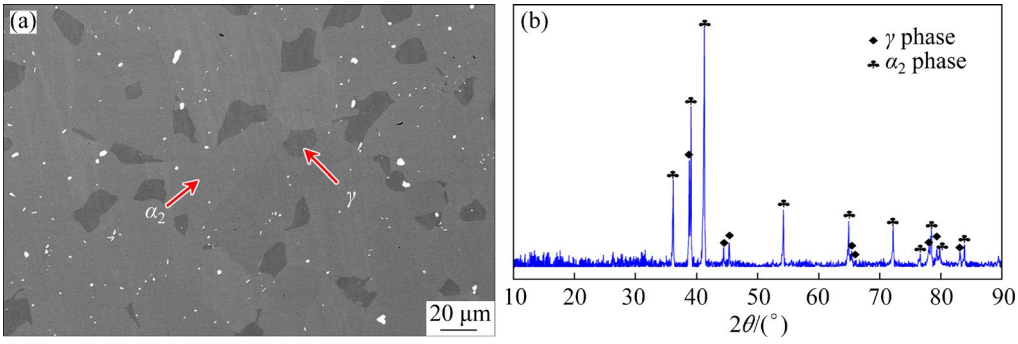

Fig. 2 Microstructure (a) and XRD pattern (b) of specimen treated at 1290 °C for 6 h and subsequently quenched in water

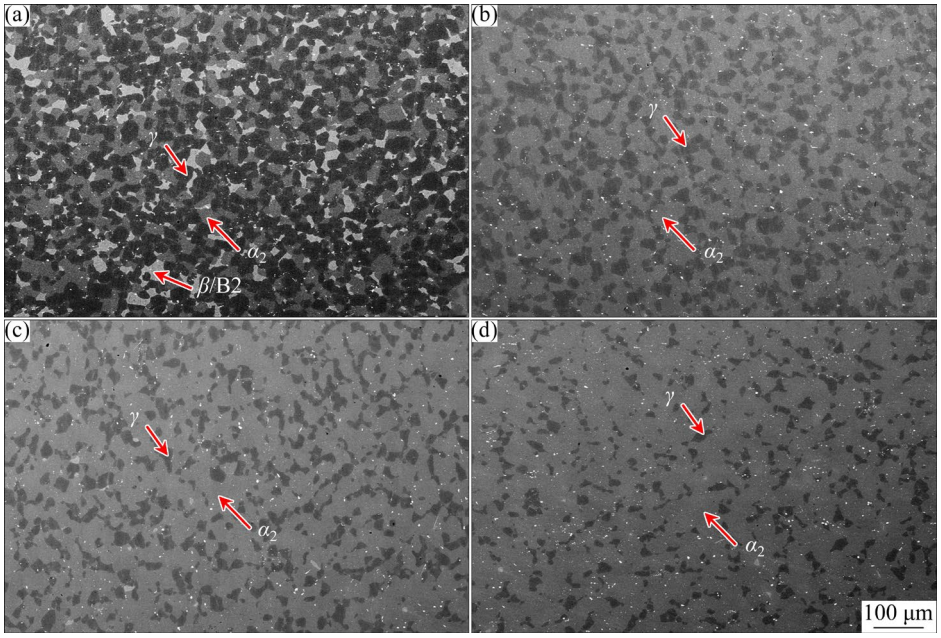

Fig. 3 Microstructures of specimen treated by different treatments: (a) 1210 °C, 12 h, WQ; (b) 1230 °C, 9 h, WQ; (c) 1250 °C, 3 h, WQ; (d) 1270 °C, 2 h, WQ

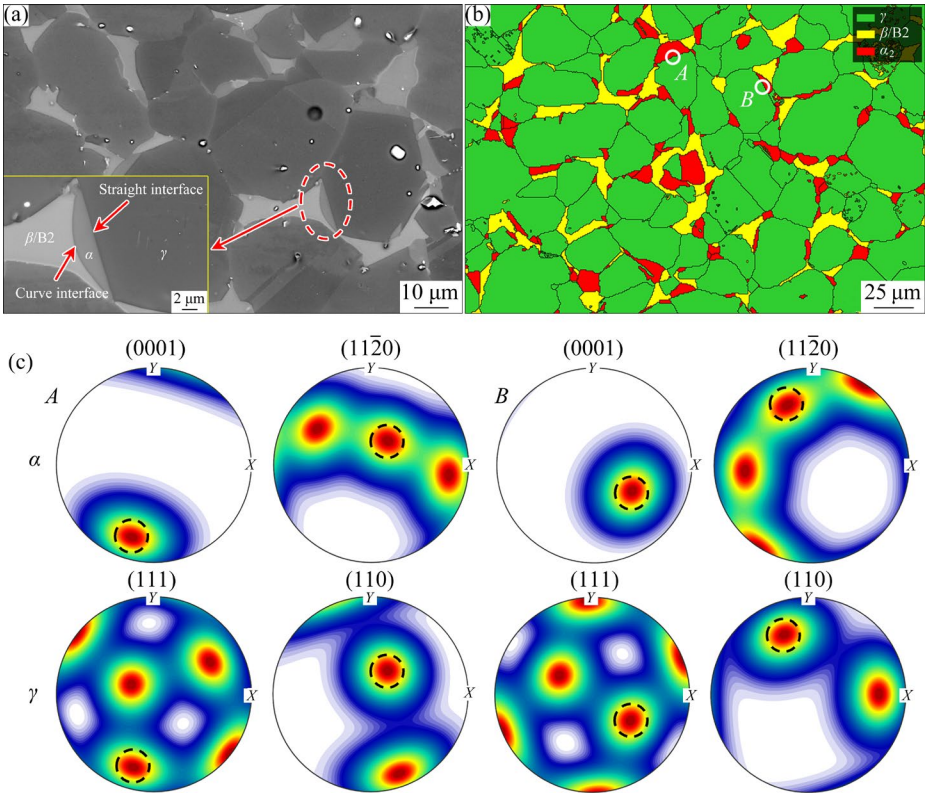

Fig. 4 BSE image (a) and phase map (b) of specimen heated at 1290 °C for 10 min followed by furnace cooling, and PF of *A* and *B* (c)

attributed to high interface energy at the phase boundary, which serves as a driving force for phase transformation, thereby reducing the nucleation work. Figure 4(a) illustrates that the α phase tends to grow into the β phase, with the interface between the γ phase and the newly formed α phase appearing relatively straight, while the interface between the β and α phases is curved. During nucleation at grain

boundary, the new phase often develops a coherent or semi-coherent cross-section with a specific grain of the parent phase, reducing both interface energy and nucleation work. The coherent side often forms a straight interface, reflecting an orientation relationship with the parent grain. As it is impossible for the crystal nucleus to maintain coherence with both adjacent grains, one side typically forms a coherent interface while the other is non-coherent, forming a spherical shape to minimize interface energy. The polar figure (PF) in Fig. 4(c) illustrates that some newly formed α phases maintain the Blackburn orientation relationship with the γ phase, specifically $(111)_\gamma//(0001)_\alpha$ and $(110)_\gamma//(11\bar{2}0)_\alpha$, indicating alignment in their crystallographic orientation.

First principles calculation was employed to calculate the formation energy of three different phases, as summarized in Table 1. The formation energy (ΔH) is calculated using the following equations:

$$\Delta H=E(V)-N_{\mathrm{Ti}}E(V)_{\mathrm{Ti}}-N_{\mathrm{Al}}E(V)_{\mathrm{Al}} \quad (1)$$

$$\Delta H_{\mathrm{a}}=\Delta H/N \quad (2)$$

where $E(V)$ is the total energy of each phase; V is the volume parameter of supercell, including six lattic parameters a, b, c, α, β and γ; $E(V)_{\mathrm{Ti}}$ and $E(V)_{\mathrm{Al}}$ are the total energy of Ti and Al, respectively; N_{Ti} and N_{Al} are the numbers of Ti and Al atoms in the structural cell, respectively; ΔH_{a} is the average formation energy per atom; N is the total number of Ti and Al atoms.

Table 1 Formation energy of different phases

Phase	Formation energy/(eV·atom^{-1})
γ-TiAl	−0.4122
α-Ti_3Al	−0.2851
B2	−0.2707

The results indicate that the formation energy of the α phase is relatively closed to that of the β phase, whereas the γ phase exhibits the lowest formation energy, suggesting a natural tendency for phase transformation between the α and β phases because of the lower energy barrier. This is coincident with the phenomena observed in Fig. 4.

This analysis demonstrates that the β phase can effectively be eliminated during the holding stage through the phase transformation of $\beta\rightarrow\alpha$. Additionally, increasing the annealing temperature accelerates the elimination of the β phase, making a high annealing temperature beneficial for complete elimination of the β phase.

Previous research on the $\beta\rightarrow\alpha$ transformation has identified three transformation modes: diffusionless martensitic mode, composition-invariant massive transformation and precipitation of the α phase from β phase [22,23]. However, the current study reveals that the α phase nucleates at the β/γ interface and grows into the adjacent β grain, maintaining a Blackburn-orientation relationship with the γ phase, though no specific orientation relationship is found between the α and β phases. This distinct phase transformation mechanism allows for the β/B2 phase to be effectively eliminated across a wide temperature range, implying potential improvements in the mechanical properties.

3.3 Formation and phase transformation of α phase

In the current alloy, the α_2 phase is absent in both the as-cast and as-forged microstructures due to the addition of large amounts of β-stabilizing elements. However, the α phase appears in the water-quenched microstructure, as shown in Figs. 2 and 3, indicating that the α phase formed during the holding stage. Figure 4 demonstrates that one route to form the α phase is $\beta\rightarrow\alpha$ phase transformation. In the water-quenched microstructure, the volume fractions of the α_2 and γ phases are 81% and 19%, respectively, whereas, in the as-forged microstructure, the volume fractions of the β/B2 and γ phases are 18% and 82%, respectively. Compared to the specimen before water quenching, the volume fraction of the γ phase remarkably decreases, while that of the α_2 phase increases markedly, and the β phase is no longer present. Figure 3 shows that, when the β/B2 phase is eliminated, the volume fractions of γ phase reduce significantly compared to the as-forged microstructure, confirming that the γ phase transforms into α phase during the holding process. With increasing annealing temperature, the α phase forms more easily, and the degree of phase transformation increases. Therefore, another route for α phase formation is the $\gamma\rightarrow\alpha$ phase transformation.

The formation and transformation of the α phase aligns with the elimination and transformation of the β/B2 phase, indicating that the elimination temperature is suitable for the formation of the α

phase. With increasing in annealing temperature, the volume fraction of the α phase also increases.

The α phase tends to grow into the β/B2 phase during phase transformation, and the analysis suggests that the primary mechanism for α phase formation is $\beta\rightarrow\alpha$ and $\gamma\rightarrow\alpha$ transformations during the holding process. In β−γ TiAl alloys, the formation of the α phase at the γ/β interface is attributed to the $\beta+\gamma\rightarrow\alpha$ transformation during the holding process [24,25]. However, this study newly reveals that the occurrence of $\beta\rightarrow\alpha$ is easier than $\gamma\rightarrow\alpha$ at the γ/β interface.

3.4 Formation of lamellar structure

The microstructure obtained after water quenching reveals equiaxed grains, as illustrated in Fig. 2(a), with the absence of a lamellar structure, suggesting that the lamellar structure forms during the cooling process. During the holding process, the primary changes are the formation and growth of the α phase.

Figure 5(a) shows the water-quenched microstructure of the specimen after heat treatment at 1290 °C for 30 min. This microstructure includes three regions, black, gray and white, presenting the γ, α_2 and β/B2 phases, respectively, with their statistical volume fractions of approximately 33%, 40%, and 27%, respectively. When the holding time is extended to 1 h, the β/B2 phase is no longer present, and the γ and α phases exhibit equiaxed morphology. The microstructure obtained by air cooling (AC) after holding at 1290 °C for 6 h is shown in Fig. 5(c), displaying equiaxed α and γ grains alongside the lamellar structure. However, the content of lamellar structure is lower compared to that in the furnace-cooled microstructure, as shown in Fig. 5(d). Hence, the result reveals that air cooling is less favorable for lamellae formation due to its faster cooling rate compared to furnace cooling (FC). Notably, no lamellar structure is found in the microstructure of the alloy when annealed for a shorter duration, demonstrating that sufficient holding time is essential for lamellae formation. In other words, the lamellar structure is formed only when the α phase reaches a certain level; otherwise, even if some α phases form, it does not easily produce a lamellar structure.

Figure 6 illustrates the lamellae formation through the growth of the α phase within the γ grains during the cooling process, represented by $L_{\alpha_2/\gamma}$. TEM analysis reveals that the lamellar structure consists of the α_2 phase alongside adjacent γ phase. The α_2 phase forms through two possible mechanisms. The first mechanism involves the initial formation of the α_2 phase at the γ grain boundary, followed by its growth within the γ grains, as depicted in Fig. 6(a). These two phases exhibit the Blackburn orientation relationship: $(111)_\gamma//(0001)_{\alpha_2}$

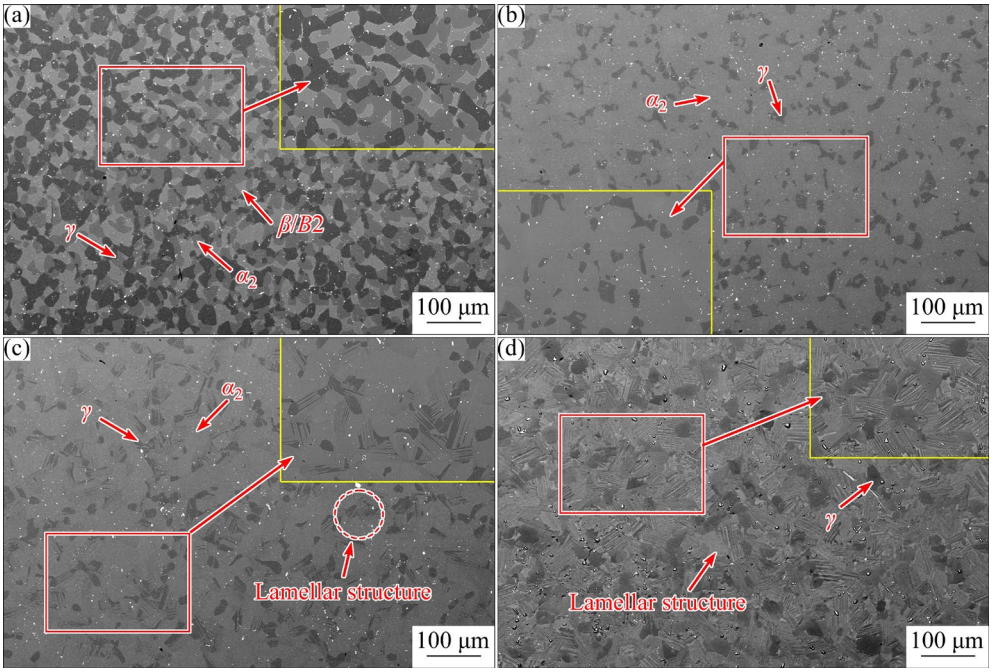

Fig. 5 Microstructures of specimen treated by different heat treatments: (a) 1290 °C, 30 min, WQ; (b) 1290 °C, 1 h, WQ; (c) 1290 °C, 6 h, AC; (d) 1290 °C, 6 h, FC

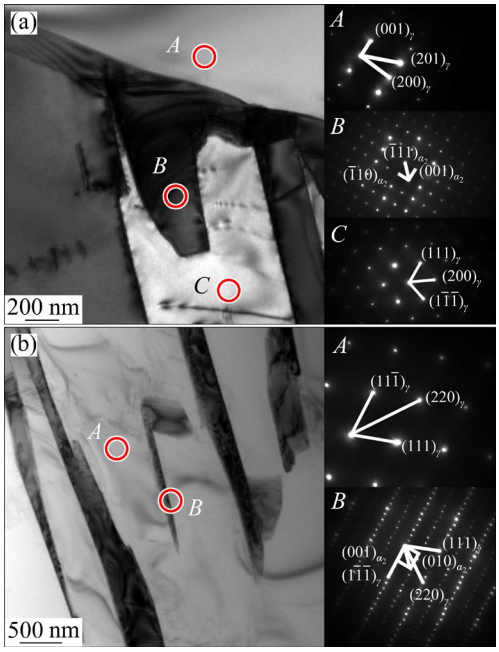

Fig. 6 (a) Growth of α phase into γ phase from grain boundary; (b) Precipitation of α phase within γ phase

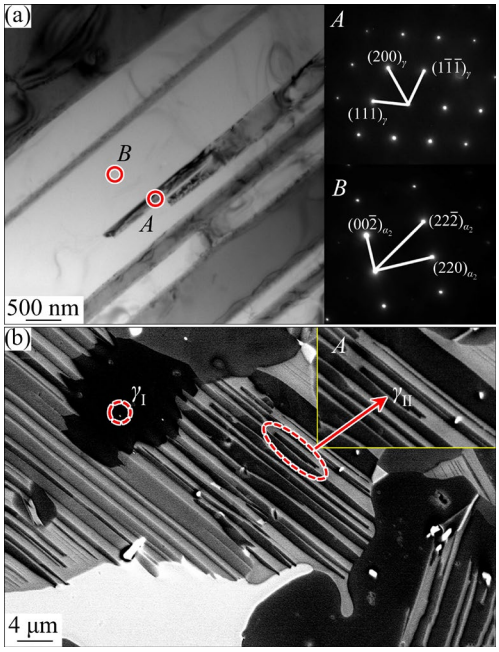

Fig. 7 (a) Growth of γ phase into α phase from grain boundary; (b) Precipitation of γ phase within α phase

and $[01\bar{1}]_\gamma // [11\bar{2}0]_{\alpha_2}$. The second mechanism, shown in Fig. 6(b), involves the α_2 phase precipitating from the γ phase and growing in both directions, contributing to the formation of the $L_{\alpha 2/\gamma}$.

A second type of lamellar structure, labelled as $L_{\gamma/\alpha 2}$, also appears in the microstructure. This lamellar structure forms as the γ phase grows within the α phase. Figure 7(a) illustrates that the γ phase nucleates at the α grain boundary and then extends into the α phase. Figure 7(b) shows a new γ phase (γ_{II}) precipitating from the α_2 phase, with γ_{II} having a composition distinct from the primary γ phase (γ_I), as detailed in Table 2. The decrease in Al content suggests that this phase transformation is diffusion-controlled. During the lamellar growth stage, more γ_{II} phases precipitate within the α phase, gradually growing throughout the α grain and eventually forming a α/γ_{II} lamellar structure.

It is suggested that the lamellar structure is formed via $\alpha \rightarrow \alpha+\gamma \rightarrow \alpha_2+\gamma$ or $\alpha \rightarrow \alpha_2 \rightarrow \alpha_2+\gamma$ transformations [26]. Figure 8 shows the water-quenched microstructures after furnace cooling from 1290 °C to different temperatures. The order−disorder transformation, $\alpha \rightarrow \alpha_2$, is controlled by the diffusion of Ti and Al atoms at the eutectoid temperature [27], which is well below 1250 °C [26,28]. When the specimen is furnace cooled to 1270 °C, both the γ and α phases exhibit equiaxed grains, with no

Table 2 Composition of different phases in lamellar structure (at.%)

Phase	Ti	Al	Nb	Mn	Cr
α_2	52.35	35.47	9.31	1.46	1.41
γ_I	46.39	44.23	8.81	–	0.57
γ_{II}	47.98	40.47	9.58	1.08	0.89

lamellar structure observed, as shown in Fig. 8(a). However, when cooled to 1260 °C, some lamellar structures start to appear and α phases precipitate from the γ phase, or some γ-laths grow within the α grains, as illustrated in Fig. 8(b). Upon furnace cooling to 1250 °C, the lamellar structure becomes prominent, with the α phase growing from the grain boundary of the γ grains or precipitating from the γ phase. These results demonstrate that the initial temperature to form the lamellar structure is around 1260 °C, which is higher than the α ordering temperature. Therefore, the lamellar structure is formed before the ordering reaction, following the phase transformation route as $\alpha \rightarrow \alpha+\gamma \rightarrow \alpha_2+\gamma$.

To observe the phase transformation more clearly, the HTLSCM was employed. Figure 9 shows the optical microstructure at various stages during heating, holding and cooling. When heated to 450 °C, the γ and β/B2 phases are clearly visible, as shown in Fig. 9(a). During the holding stage, the α phase

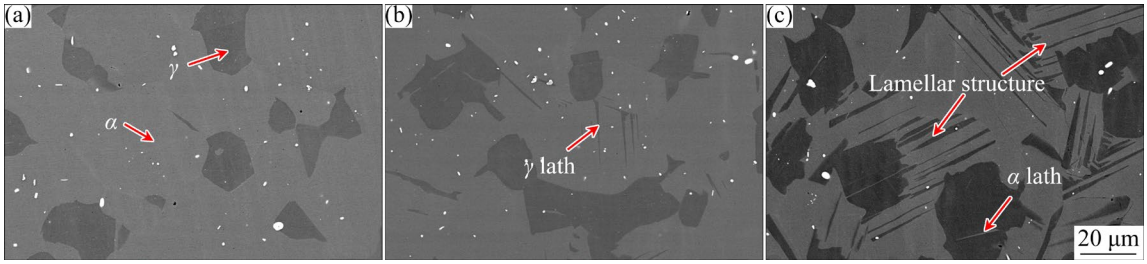

Fig. 8 Microstructures of as-forged alloy treated at 1290 °C for 6 h, and then furnace cooled to 1270 °C (a), 1260 °C (b) and 1250 °C (c), followed by water quenching

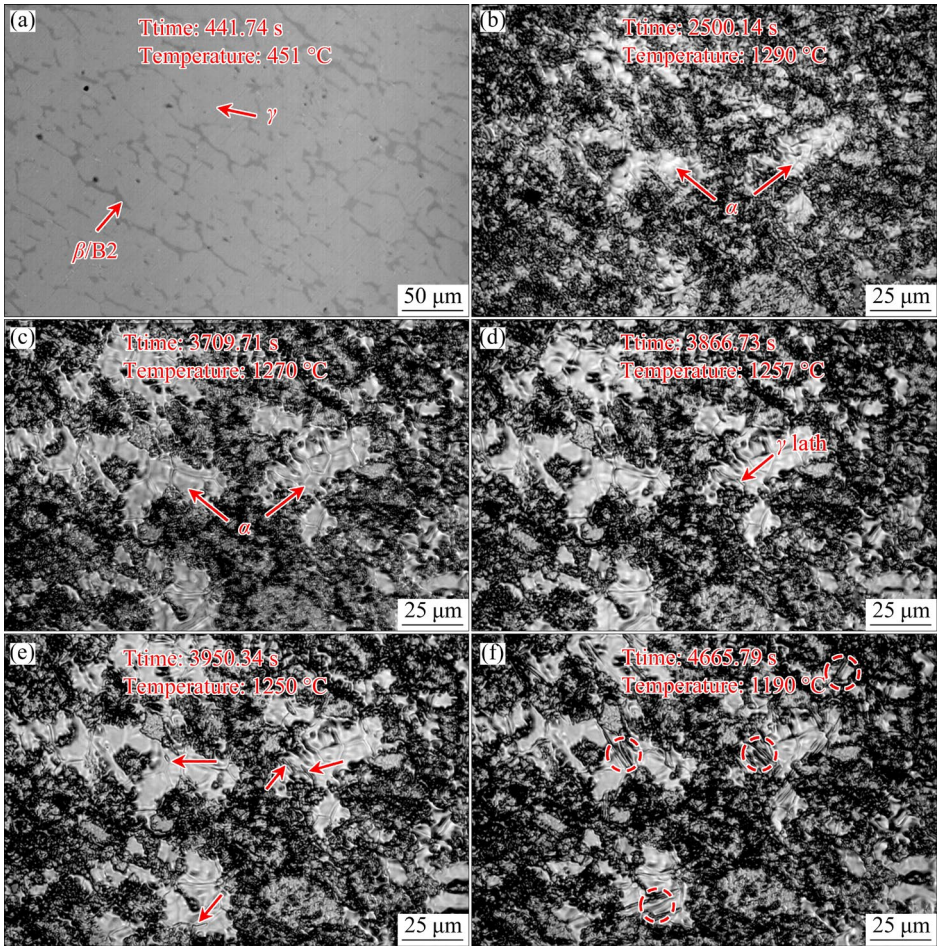

Fig. 9 Optical microstructures of specimen observed by HTLSCM at different stages: (a) Heated to 450 °C; (b) Held at 1290 °C; (c−f) Cooled to 1270, 1257, 1250 and 1190 °C from 1290 °C, respectively

progressively forms and grows with increasing the holding time, as illustrated in Fig. 9(b). In the furnace cooling stage, no lamellar structure was identified prior to 1260 °C. Figure 9(c) reveals the optical microstructure at 1270 °C. The new α grains exhibit equiaxed morphology, with no lamellar structure present. The microstructure remains relatively unchanged until the temperature cools to 1260 °C. Once the temperature drops to 1257 °C, the γ lath begins to form at the grain boundary of the α grain, marked by the red arrow in Fig. 9(d). As the temperature continues to drop, more γ laths bud and grow, as seen in Figs. 9(e) and (f). The lamellar structure then forms through the growth of these laths.

It should be noted that the initial formation temperature of the lamellar structure aligns with the result of the water-quenched experiments. At the annealing temperatures of 1270 and 1250 °C, the formation temperatures for the lamellar structure are

approximately 1230 and 1210 °C, respectively. These results indicate that the formation temperature of the lamellar structure is 30−40 °C below the annealing temperature.

As depicted in Fig. 10, equiaxed α grains and several laths are visible in the microstructure observed through HTLSCM. Based on the heat treatment results, these laths are identified as γ laths. It is evident that these γ laths nucleate at the grain boundaries of α grains (Fig. 10(a)) and precipitate within the α grains (Fig. 10(b)). Notably, $L_{\alpha_2/\gamma}$ is not observed, suggesting that L_{γ/α_2} is the predominant lamellar structure. The microstructure in Fig. 8(c) further shows a higher content of L_{γ/α_2} compared to $L_{\alpha_2/\gamma}$.

The lamellar structure, formed by the alternating growth of the α and γ phases, is shown in Fig. 11. This structure consists of alternating γ and α phases. with an orientation relationship of $(111)_\gamma // (0001)_\alpha$ and $[01\bar{1}]_\gamma // [11\bar{2}0]_\alpha$. Figure 11(b) presents a high-resolution TEM (HRTEM) image of the interface between γ and the α phases within the lamellar structure. Calculations show that the crystal plane spaces of $(111)_\gamma$ and $(002)_\alpha$ are 0.2325 and 0.2365 nm, respectively. The lattice mismatch between $(111)_\gamma$ and $(002)_\alpha$ is only 1.7%, confirming that the γ lath possesses a coherent relationship with the α lath, and that the interface is well integrated.

The TKD analysis of the lamellar structure is shown in Fig. 12. Two types of interfaces emerge from the lamellar structure: the γ/α_2 interface and the γ/γ interface. The α laths within the same lamellar colony share the same orientation, while some adjacent γ laths display different orientations, as marked by the arrows in Fig. 12(b). The boundaries between these adjacent γ-laths are identified as Σ3 grain boundaries: [110] 70°, classifying them as twin boundaries. The γ phase has a tetragonal structure (c/a≈1.02), hence there are three different types of the γ/γ interfaces: true-twin boundary (TT), pseudo-twin boundary (PT), and rotation boundary (RB) [29]. The [110] 70° boundary represents the true-twin boundary [30]. The occurrence of the TT interface can be explained by the minimization of the elastic energy of the interfaces [31]. From the phase map (Fig. 12(a)), it can be observed that the γ phase precipitates from the α phase, as indicated by the cycle. This result suggests that precipitation and growth of the α and the γ phases not only form the lamellar structure during the formation stage but also help refine the lamellar spacing. The polar figure of the adjacent γ and α laths proves that these two phases follow a crystallography relationship:

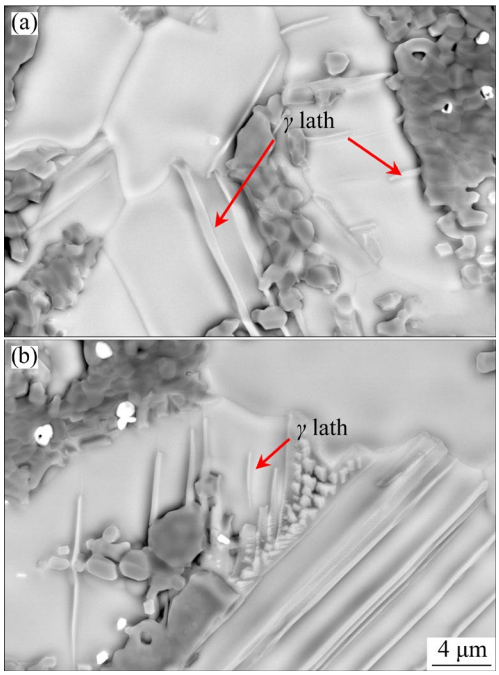

Fig. 10 Microstructures of sample after HTLSCM test: (a) γ lath growing from grain boundary; (b) γ lath in grains

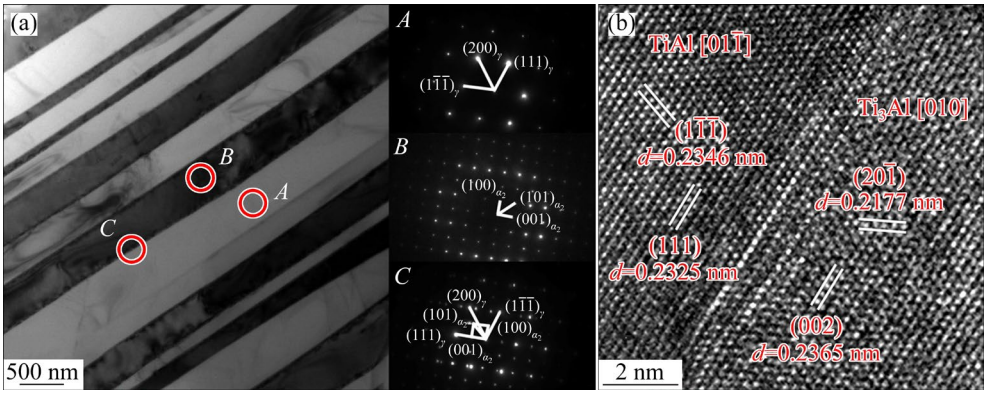

Fig. 11 Characterization of lamellar structure: (a) TEM image; (b) HRTEM image of γ/α interface

$(111)_\gamma//(0001)_\alpha$ and $(110)_\gamma//(11\bar{2}0)_\alpha$. This relationship is also applicable to the precipitated γ phase and the α phase, consistent with TEM result shown in Fig. 11(a) and other reports [8].

In the current TiAl alloy, the mechanism of the lamellae formation involves two types: growth from grain boundaries and intragranular precipitation. Figure 13 presents the schematic illustration of lamellae formation, demonstrating three stages. In the first stage, the phase transformations of $\beta\rightarrow\alpha$ and $\gamma\rightarrow\alpha$ take place preferentially, with the α phase nucleating at the boundaries of the β and γ phases. The new α and γ phases exhibit a coherent relationship and grow within the β phase. In the

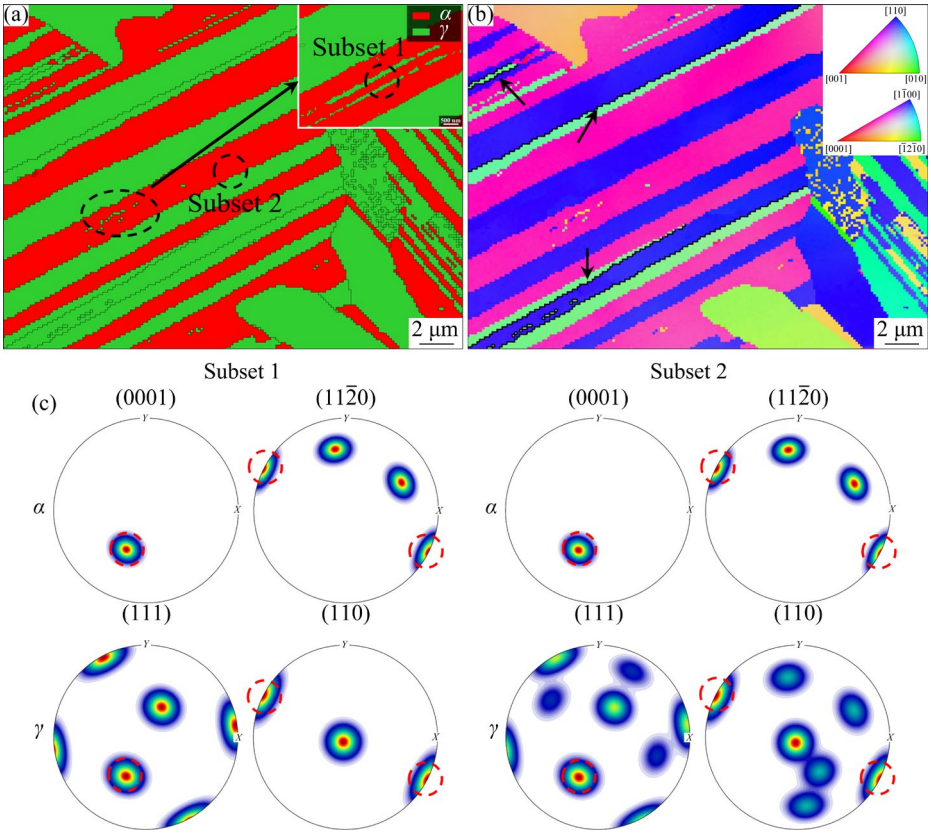

Fig. 12 TKD characterization of lamellar structure: (a) Phase map; (b) IPF; (c) Polar figure

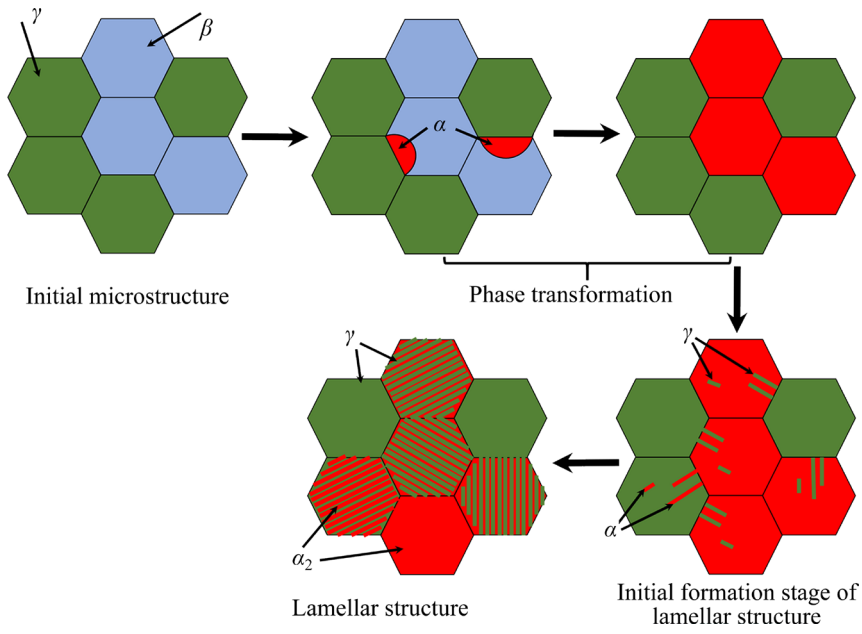

Fig. 13 Schematic illustration of lamellae formation

second stage, nucleation or precipitation of the α and γ phases occurs, followed by their growth. The final stage involves the growth of the lamellar structure.

In TiAl alloys containing α and γ phases, the formation of γ lamellae starts within the α+γ phase field and is completed in the α_2+γ phase field, with the γ phase nucleating within the α matrix [15]. The laths formed at the γ grain boundary can occur at any temperature in the α+γ phase field, while the lath formation within the γ grains requires higher temperature [16]. In contrast, the formation of the lamellar structure in this study follows a different mechanism. The $\beta\rightarrow\alpha$ phase transformation is essential before the lamellae formation, and a sufficient amount of newly formed α phase is required for lamellae formation. Additionally, the γ laths form not only within the α grains, but also at the α grain boundaries, and the α-laths can form both at the γ grain boundary and within the interior of γ grain.

4 Conclusions

(1) The elimination of the β phase and the formation of the α phase occur during the holding process of annealing, with the primary phase transformation being $\beta\rightarrow\alpha$ and $\gamma\rightarrow\alpha$. As the annealing temperature increases, the time required for the $\beta\rightarrow\alpha$ transformation decreases.

(2) The lamellar structure forms during furnace cooling and requires sufficient holding time. The initial formation temperature of the lamellar structure is 30−40 °C lower than the annealing temperature.

(3) Two main mechanisms are identified for the formation of the lamellar structure: growth from the grain boundary and intragranular precipitation. The first mechanism involves nucleation at the grain boundary followed by growth into the grains, while the second one entails precipitation and growth within the grains.

(4) The relationship between the γ and α_2 phases in the lamellar structure follows the orientation relationship: $(111)_\gamma//(0001)_{\alpha 2}$ and $[01\bar{1}]_\gamma//[11\bar{2}0]_{\alpha_2}$. The interface between the two phases is coherent, with a misfit of about 1.7%.

CRediT authorship contribution statement

Geng-wu GE: Investigation, Methodology, Writing − Original draft, Writing − Review & editing; **Lai-qi ZHANG:** Conceptualization, Methodology, Funding acquisition; **Jun-pin LIN:** Writing − Review & editing.

Declaration of competing interest

The authors declare that they have no known competing financial interests or personal relationships that could have appeared to influence the work reported in this paper.

Acknowledgments

This work was supported by the National Natural Science Foundation of China (Nos. 51871012, 52071021), Beijing Natural Science Foundation, China (No. 2162024), Fundamental Research Funds for the Central Universities, China (No. FRF-GF-20-20B), and the National Program on Key Basic Research Project of China (No. 2011CB605502).

References

[1] KIM Y W, KIM S L. Advances in gammalloy materials−processes−application technology: Successes, dilemmas, and future [J]. JOM, 2018, 70(4): 553−560.

[2] MAYER S, ERDELY P, FISCHER F D, HOLEC D, KASTENHUBER M, KLEIN T, CLEMENS H. Intermetallic β-solidifying γ-TiAl based alloys−From fundamental research to application [J]. Advanced Engineering Materials, 2017, 19(4): 1600735.

[3] CHEN Guang, PENG Ying-bo, ZHENG Gong, QI Zhi-xiang, WANG Min-zhi, YU Hui-chen, DONG Cheng-li, LIU C T. Polysynthetic twinned TiAl single crystals for high-temperature applications [J]. Nature Materials, 2016, 15: 876−881.

[4] SONG L, APPEL F, WANG Li, OEHRING M, HU Xing-guo, STARK A, HE Jun-yang, LORENZ U, ZHANG Tie-bang, LIN Jun-pin, PYCZAK F. New insights into high-temperature deformation and phase transformation mechanisms of lamellar structures in high Nb-containing TiAl alloys [J]. Acta Materialia, 2020, 186: 575−586.

[5] CUI Ning, KONG Fan-tao, WANG Xiao-peng, CHEN Yu-yong, ZHOU Hai-tao. Hot deformation behavior and dynamic recrystallization of a β-solidifying TiAl alloy [J]. Materials Science and Engineering: A, 2016, 652: 231−238.

[6] JIANG Hai-tao, ZENG Shang-wu, ZHAO Ai-min, DING Xiao-nan, DONG Peng. Hot deformation behavior of β phase containing γ-TiAl alloy [J]. Materials Science and Engineering: A, 2016, 661: 160−167.

[7] XIAO Shu-long, CHEN Yu-yong, LI Ming-ao, XU Li-juan, TIAN Jing, ZHANG Dong-dong, YANG Jian-hui. The improved properties and microstructure of β-solidify TiAl alloys by boron addition and multi steps forging process [J]. Scientific Reports, 2019, 9(1): 12393.

[8] APPEL F, PAUL J D H, OEHRING M. Gamma titanium aluminide alloys: Science and technology [M]. Weinheim: John Wiley & Sons, 2011.

[9] LI Xiao-bing, XU Hao XU, XING Wei-wei, CHEN Bo, SHU Lei, ZHANG Meng-shu, LIU Kui. Microstructural evolution and mechanical properties of forged β-solidified γ-TiAl alloy by different heat treatments [J]. Transactions of Nonferrous Metals Society of China, 2022, 32(7): 2229−2242.

[10] ZHU Dong-dong, YAN Jiang-fei, JIN Yu-liang, DONG Duo, WANG Xiao-hong, MA Teng-fei. Pressure-induced excellent corrosion resistance of Ti−45Al−8Nb alloy [J]. Materials Letters, 2024, 355: 135446.
[11] ZHENG Guo-ming, TANG Bin, ZHAO Song-kuan, WANG W Y, CHEN Xiao-fei, ZHU Lei, LI Jin-shan. Evading the strength-ductility trade-off at room temperature and achieving ultrahigh plasticity at 800 ℃ in a TiAl alloy [J]. Acta Materialia, 2022, 225: 117585.
[12] LI Ying, ZHOU Lian, LIN Jun-pin, CHANG Hui, LI Feng. Phase transformation behavior and kinetics of high Nb−TiAl alloy during continuous cooling [J]. Journal of Alloys and Compounds, 2016, 668: 22−26.
[13] KLEIN T, NIKNAFS S, DIPPENAAR R, CLEMENS H, MAYER S. Grain growth and β to α transformation behavior of a β-solidifying TiAl alloy [J]. Advanced Engineering Materials, 2015, 17(6): 786−790.
[14] QIANG Feng-ming, KOU Hong-chao, WANG Ling-ling, LI Jin-shan. β_o precipitation in α_2 lamellae of the β-solidifying multiple-phase γ-TiAl alloy [J]. Materials Characterization, 2020, 167: 110474.
[15] DENQUIN A, NAKA S. Phase transformation mechanisms involved in two-phase TiAl-based alloy: I. Lamellar structure formation [J]. Acta Materialia, 1996, 44(1): 343−352.
[16] KUMAGAI T, ABE E, KIMURA T, NAKAMURA M. The $\gamma\rightarrow\alpha$ phase transformation in γ-based TiAl alloy [J]. Scripta Materialia, 1996, 34(2): 235−242.
[17] GE Geng-wu, WANG Ze-ming, LIANG Si-yuan, ZHANG Lai-qi. Achievement of forging without canning for β-solidifying γ-TiAl alloy containing high content of niobium [J]. Materials and Manufacturing Processes, 2021, 36(14): 1667−1676.
[18] ZHANG Lai-qi, GE Geng-wu, LIN Jun-pin, AINDOW M, ZHANG Li-chun. Effect of transition metal alloying elements on the deformation of Ti−44Al−8Nb−0.2B−0.2Y alloys [J]. Scientific Reports, 2018, 8(1): 14242.
[19] BACHMANN F, HIELSCHER R, SCHAEBEN H. Texture analysis with MTEX-free and open source software toolbox [J]. Solid State Phenomena, 2010, 160: 63−68.
[20] ERDELY P, WERNER R, SCHWAIGHOFER E, CLEMENS H, MAYER S. In-situ study of the time–temperature-transformation behaviour of a multi-phase intermetallic β-stabilised TiAl alloy [J]. Intermetallics, 2015, 57: 17−24.
[21] KARTAVYKH A V, ASNIS E A, PISKUN N V, STATKEVICH I I, STEPASHKIN A A, GORSHENKOV M V, AKOPYAN T K. Complementary thermodynamic and dilatometric assessment of phase transformation pathway in new β-stabilized TiAl intermetallics [J]. Materials Letters, 2017, 189: 217−220.
[22] YAMABE Y, TAKEYAMA M, KIKUCHI M. Microstructure evolution through solid-solid phase transformations in gamma titanium aluminides [C]//Gamma Titanium Aluminides. Warrendale: TMS, 1995: 111−129.
[23] BANERJEE S, MUKHOPADHYAY P. Phase transformations: Examples from titanium and zirconium alloys [M]. Amsterdam: Elsevier, 2010.
[24] WU Yu-lun, HU Rui, YANG Jie-ren, XUE Xiang-yi. Phase transformation and fine fully lamellar (FFL) structure formation in a high Nb-containing beta-gamma TiAl alloy [J]. Advanced Engineering Materials, 2019, 21(8): 1900244.
[25] HUANG Hao-tao, DING Hong-sheng, XU Xue-song, CHEN Rui-run, GUO Jing-jie, FU Heng-zhi. Phase transformation and microstructure evolution of a beta-solidified gamma-TiAl alloy [J]. Journal of Alloys and Compounds, 2021, 860: 158082.
[26] JONES S A, KAUFMAN M J. Phase equilibria and transformations in intermediate titanium aluminum alloys [J]. Acta Metallurgica et Materialia, 1993, 41(2): 387−398.
[27] OHNUMA I, FUJITA Y, MITSUI H, ISHIKAWA K, KAINUMA R, ISHIDA K. Phase equilibria in the Ti−Al binary system [J]. Acta Materialia, 2000, 48(12): 3113−3123.
[28] YAMABE Y, TAKEYAMA M, KIKUCHI M. Determination of α(A3)→α_2 (D0$_{19}$) transition temperatures in Ti−(40−45)at% Al alloys [J]. Scripta Metallurgica et Materialia, 1994, 30: 553−557.
[29] CHEN S H, SCHUMACHER G J S M. The application of transformation matrices on the determination of γ/γ interface types in a γ-TiAl alloy [J]. Scripta Materialia, 2004, 50(1): 31−34.
[30] ZONG Ying-ying, WEN Dao-sheng, LIU Zu-yan, SHAN De-bin. γ-phase transformation, dynamic recrystallization and texture of a forged TiAl-based alloy based on plane strain compression at elevated temperature [J]. Materials & Design, 2016, 91: 321−330.
[31] ZGHAL S, NAKA S, COURET A. A quantitative TEM analysis of the lamellar microstructure in TiAl based alloys [J]. Acta Materialia, 1997, 45(7): 3005−3015.

锻造 β 凝固高 Nb−TiAl 合金在退火过程中的相变和片层形成

葛庚午，张来启，林均品

北京科技大学 新金属材料全国重点实验室，北京 100083

摘　要：采用不同热处理制度研究了含 β/B2 和 γ 相的 β 凝固高 Nb−TiAl 合金中 B2 相的消除，并研究了该过程中的相变和片层形成。B2 相消除过程中的相变行为和片层组织的形成规律与传统 TiAl 合金存在差异。在热处理保温阶段，通过 $\beta\rightarrow\alpha$ 和 $\gamma\rightarrow\alpha$ 的初始相变，β/B2 相被 α 相取代。冷却过程中 α 和 γ 晶粒内均形成片层结构，其初始形成温度比退火温度低 30~40 ℃。这种片层结构的形成机制主要有 2 种，即在晶界处形核并向晶内生长和晶内直接析出并长大。片层结构中 γ 相和相邻的 α 相的取向关系为$(111)_\gamma//(0001)_\alpha$和$[01\bar{1}]_\gamma//[11\bar{2}0]_{\alpha_2}$，且两者为共格关系，错配度约为 1.7%。

关键词：β 凝固高 Nb−TiAl 合金；热处理；相变；片层结构

(Edited by Xiang-qun LI)